

ASCA Observations of the Central Regions of M31

Hiromitsu TAKAHASHI, Yuu OKADA, Motohide KOKUBUN, and Kazuo MAKISHIMA
Department of Physics, University of Tokyo, 7-3-1 Hongo, Bunkyo-ku, Tokyo 113-0033
hirotaka@amalthea.phys.s.u-tokyo.ac.jp

(Received 2001 April 26; accepted 2001 August 21)

Abstract

Using ASCA, spatially integrated X-ray spectra of the central regions of M31 were studied. Data were accumulated over three different circular regions, with the radii of 3', 6' and 12', all centered on the nucleus. The spectra are relatively similar among the three regions. In the energy range above 1.5 keV, the spectra are reproduced by a combination of a disk black-body component and a black-body component, implying that the emission mainly comes from an assembly of low-mass X-ray binaries. In energies below 1.5 keV, the spectra involves two additional softer components, expressed with thin-thermal plasma emission models of temperatures ~ 0.9 keV and ~ 0.3 keV. Over the central 12' (2.4 kpc) region and in the 0.5–10 keV energy band, the binary component has a luminosity of 2.6×10^{39} erg s $^{-1}$, while the two softer components both exhibit luminosities of $\sim 2 \times 10^{38}$ erg s $^{-1}$. These results are compared with those from other missions, including Chandra and XMM-Newton in particular. Discussion is made on the nature of the two softer spectral components besides the binary one.

Key words: galaxies: individual (M31) — galaxies: spiral — X-rays: galaxies

1. Introduction

M31, the Andromeda Nebula, is the nearest (~ 700 kpc) spiral galaxy, forming the Local Group of galaxies together with our Milky Way and others. Its close distance enables us to perform very detailed observations in the X-ray band. Because the direction to M31 is clear of strong absorption along the Galactic plane, it potentially allows more comprehensive X-ray spectroscopic studies of X-ray sources over a wider energy range than is possible for those in our own Galaxy.

Consequently, many X-ray observations of M31 were so far performed. The soft X-ray maps of M31 obtained by Einstein and ROSAT respectively revealed over 100 sources with the 0.2–4.0 keV luminosity exceeding 5×10^{36} erg s $^{-1}$ (Trinchieri & Fabbiano 1991), and more than 300 sources with the 0.1–2.4 keV luminosity exceeding 3×10^{35} erg s $^{-1}$ (Supper et al. 1997). In the hard 2–20 keV energy band, the integrated spectrum of the galaxy obtained with Ginga has been understood as emission from a collection of X-ray binaries, with the integrated luminosity reaching $\sim 5 \times 10^{39}$ erg s $^{-1}$ (Makishima et al. 1989b; hereafter Paper I).

The Einstein and ROSAT observations also revealed unresolved and apparently extended X-ray emission from the bulge of M31. This is thought to be emission from a diffuse hot plasma, or from a collection of faint discrete sources below the detection limit (Trinchieri & Fabbiano 1991; Primini et al. 1993; Supper et al. 1997; West et al. 1997; Irwin & Bregman 1999b; Borozdin & Priedhorsky 2000). Using the BeppoSAX spectra, Trinchieri et al. (1999) reconfirmed that the hard-band ($\gtrsim 2$ keV) emission from M31 can be described by a collection of binary sources, while an additional spectral component is required in the soft band. However, due to the limited energy resolution in the soft band, the properties of the additional soft emission remains poorly understood. A further confusion as to the nature of the soft component is caused by uncertainties in the way of modeling the X-ray binary spectra below ~ 1.5 keV (e.g., Irwin & Bregman 1999b; Trinchieri et al. 1999), which persist even in the latest studies with Chandra and XMM-Newton (Primini et al. 2000; Garcia et al. 2000b; Shirey et al. 2001).

To study this unresolved emission, we analyzed the integrated 0.6–10 keV spectra of the central (up to 2.4 kpc) regions of M31 taken with the GIS (Gas Imaging Spectrometer; Ohahi et al. 1996; Makishima et al. 1996) and the SIS (Solid-state Imaging Spectrometer; Burke et al. 1991; Gendreau et al. 1993; Yamashita et al. 1997), both onboard ASCA (Tanaka et al. 1994). By employing a physical modeling of the X-ray binary spectra established through observations of Galactic X-ray sources (Mitsuda et al. 1984; Makishima et al. 1989a; Asai et al. 2000), we have discovered that the unresolved soft emission involves two plasma temperatures, ~ 0.9 keV and ~ 0.3 keV. Therefore, the unresolved emission is likely to consist of two distinct components.

2. Observation and Data Reduction

The ASCA observations of M31 were performed from 28 to 31 July 1993 in the performance verification phase for ~ 120 ks in total. The observations were divided into six partially-overlapping pointings covering a large fraction of the optical galaxy disk, including the central region in particular. During all these observations, the GIS was operated in normal pulse-height mode, and the SIS was in 4CCD mode. In figure 1, we show the mosaic GIS images from all the six pointings. Thus, the central region of M31 is too crowded to be resolved by ASCA. In the present paper, we therefore analyze the data from this central-pointing field as a collection of many discrete sources and possibly diffuse emission, in an attempt to separate different X-ray components spectrally rather than spatially.

For the central pointing data, we screened the events under the condition of a telescope viewing direction of $> 5^\circ$ from the dark Earth rim, and a magnetic cutoff rigidity > 8 GV and > 6 GV for the GIS and the SIS, respectively. For the SIS data, we further required the time after day-night transition to be > 100 s, and the elevation angle from the sunlit Earth rim to be $> 30^\circ$ in order to avoid the effect of light leakage on the CCD chips. We also removed particle events by the standard rise-time rejection for the GIS, and similarly removed hot or flickering pixels for the SIS. After applying these criteria, we obtained net exposures of ~ 21 ks with the GIS (GIS2+GIS3) and ~ 14 ks with the SIS (SIS0+SIS1). The 0.7–10 keV count rates were ~ 0.9 c s $^{-1}$ and ~ 1.1 c s $^{-1}$, for the GIS and SIS, respectively.

3. Data Analysis and Results

3.1. Accumulation of Energy Spectra

After the data screening described in section 2, we constructed the GIS and SIS energy spectra for the central region of M31. The events were extracted from a circular region centered on the nucleus, using a radius of 12' (2.4 kpc), the largest possible radius without being affected by dominant point sources which should be analyzed individually. As to the SIS, the field of view (22' \times 22' in 4CCD mode) is a little smaller than the 12' radius, and we use only the region on the detector. We derived background data from blank-sky observations, for which we applied the same data-selection criteria as in section 2, and used the same photon-accumulation region. After the background subtractions and appropriate gain corrections, we added the data from GIS2 and GIS3 into a single GIS spectrum, and those from SIS0 and SIS1 into a single SIS spectrum. The obtained spectra are shown in figure 2 without removing the instrumental responses. The signal X-rays are thus detected over the 0.7–10 keV range with the GIS, and over the 0.6–7.5 keV range with the SIS.

In order to roughly investigate the spatial distribution of X-ray sources, we also accumulated two more pairs of spectra over smaller circular regions centered on the nucleus, using radii of 3' (0.6 kpc) and 6' (1.2 kpc). The former radius is twice as large as the half-power radius of ASCA. Below, we analyze the 12' spectra in subsections 3.2 through 3.4, and apply the results to the 3' and 6' ones in subsection 3.5.

3.2. Modeling of the 1.5–10 keV Spectra

The X-ray emission from M31 is thought to be dominated by a collection of low-mass X-ray binaries (LMXBs, accreting binaries involving neutron stars with weak magnetic fields) at least in energy bands above ~ 1.5 keV (Paper I; Trinchieri et al. 1999; Shirey et al. 2001). Indeed, when the absorption was fixed to the Galactic value along the line of sight toward M31, $N_{\text{H}} = 6.7 \times 10^{20}$ cm $^{-2}$ (from Einline and W3nH), the 2–20 keV spectrum of the whole M31 obtained with Ginga has been described successfully (Paper I) by the physical model developed for Galactic high-luminosity LMXBs; it consists of a disk black-body (DBB) component and a black-body (BB) component, which represent emission from the optically-thick accretion disk and the central neutron star, respectively (Mitsuda et al. 1984; Makishima et al. 1989a; Asai et al. 2000). We hereafter refer to this model as the LMXB model (see Appendix for detail). In contrast, the Ginga spectrum was not reproduced by thermal Bremsstrahlung or power-law models, unless a significant amount of excess absorption was incorporated. Since the absorption within M31 itself is rather small, the excess absorption is considered artificial, making these two alternative spectral models unrealistic.

We accordingly fitted the 1.5–10 keV GIS and SIS spectra of the central 12' radius simultaneously with the LMXB model. Here and hereafter, we fix the value of the absorption column density at the Galactic value. As summarized in table 1, the LMXB model has simultaneously reproduced the GIS/SIS spectra very well in the energy range above 1.5 keV, and the obtained parameters are consistent with those obtained previously with Ginga (Paper I). Furthermore, the inner-disk temperature of $kT_{\text{in}} \sim 1.0$ keV, the BB temperature of $kT_{\text{BB}} \sim 2.0$ keV, and the cross-over of the two components at 3.3 keV (figure 2), are all typical of luminous Galactic and Magellanic LMXBs (Mitsuda et al. 1984). It is therefore reconfirmed that a collection of LMXBs dominates the X-ray emission from M31 above ~ 1.5 keV. In subsection 3.6, we examine what happens if our LMXB model is replaced with more conventional ones, such as a single thermal Bremsstrahlung or a single power-law model, even though these alternative modelings have already been ruled out by Ginga (Paper I).

3.3. Inclusion of the 0.8–1.5 keV Energy Band

When the best-fit LMXB model determined in the 1.5–10 keV band is extrapolated toward lower energies, the model prediction falls significantly short of the actual data (figure 2); the fit actually becomes unacceptable by including the 0.8–1.5 keV band, even re-adjusting the model parameters except N_{H} (table 1). This reconfirms the previous reports on the soft X-ray excess (Irwin & Bregman 1999b; Trinchieri et al. 1999; Borozdin & Priedhorsky 2000; Shirey et al. 2001). The soft excess is consistently seen between the two ASCA instruments, although it is more significant in the SIS data because of its improved low-energy efficiency.

We suspect the soft excess, prominent below energies of ~ 1 keV in figure 2, to be contributed significantly by low-energy atomic lines emergent from thin-thermal plasmas. We accordingly examined the 0.8–3.5 keV portion of the GIS/SIS spectra more closely for the existence of atomic emission lines from major elements. We approximated the overall GIS/SIS continua (including the soft excess) conventionally by a single Bremsstrahlung model, to find a rather poor fit with $\chi^2/\text{d.o.f.} = 351/227$ as shown in figure 3a. By including 5 Gaussians, in contrast, the fit has been significantly improved ($\chi^2/\text{d.o.f.} = 211/217$; figure 3b). The five Gaussians are centered at $0.82^{+0.02}_{-0.01}$ keV, $0.93^{+0.01}_{-0.02}$ keV, $1.03^{+0.01}_{-0.02}$ keV, $1.85^{+0.06}_{-0.05}$ keV, and 2.26 ± 0.04 keV, with equivalent widths of 49^{+10}_{-12} eV, 36^{+10}_{-13} eV, 38^{+11}_{-8} eV, 15 ± 11 eV, and 44^{+11}_{-25} eV, respectively. Thus, the lines are statistically significant. Based on the central energies, the former three lines may be assigned to either ionized Ne-K or ionized Fe-L lines, while the latter two to ionized Si-K and S-K lines, respectively. We can hence conclude that the spectra exhibit statistically significant evidence of low-energy emission lines from ionized abundant heavy elements.

Now that the thin-thermal nature of the soft excess has been confirmed, we are justified to express the soft excess by a thin-thermal plasma emission model. Specifically, we employ the Raymond-Smith emission model (Raymond & Smith 1977; hereafter RS model), and tentatively fix its metal abundance at 1.0 solar, as has been found from the Galactic ridge emission (Kaneda et al. 1997; Valinia & Marshall 1998) and an apparently diffuse X-ray emission filling the Galactic bulge (Kokubun 2001). We hence fitted the GIS/SIS spectra over the 0.8–10 keV energy band by the sum of the LMXB and RS components. This two-component model, denoted LMXB+RS model, has successfully explained the 0.8–10 keV GIS/SIS spectra, with the plasma temperature being ~ 0.8 keV (table 1). In other words, the soft excess seen in figure 2 below 1.5 keV has been explained successfully as emission from a 0.8 keV thin-thermal plasma.

3.4. Inclusion of the 0.6–0.8 keV Energy Band

As in subsection 3.3, we extended the LMXB+RS model, determined over the 0.8–10 keV energy band, further into the 0.6–10 keV energy band. Then, as shown in figure 4, the model has again left a large excess below ~ 0.8 keV. As a result, the LMXB+RS fit that was acceptable in the 0.8–10 keV range becomes unacceptable in the 0.6–10 keV range, even re-adjusting the model parameters except N_{H} and abundances (table 1). This indicates the presence of a third, and the softest, emission component that dominates the spectra below ~ 0.8 keV.

The softest component may be contributed by O-K lines appearing in the 0.6–0.7 keV range. We therefore added one more RS component to jointly fit the total-band (0.6–10 keV) GIS/SIS spectra. This model, denoted LMXB+2RS model, has indeed decreased χ^2 down to an acceptable level, as shown in figure 5 and table 1. The obtained two plasma temperatures are ~ 0.9 keV and ~ 0.3 keV, and their luminosities are given in table 3; here and hereafter, we quote luminosities in the 0.5–10 keV energy band. Even if the metal abundances of the two RS components are allowed to vary freely, the fit result does not change significantly, and neither of the two RS components vanishes. If, for simplicity, we constrain the two RS components to have common abundances with solar ratios, the 90% confidence range of the metal abundance becomes ≥ 0.09 solar. When the MEKAL model (Mewe et al. 1985, 1986; Kaastra 1992; Liedahl et al. 1995) is used instead of the RS model, the spectra also require two thin-thermal components besides the LMXB component, and the obtained parameters are consistent, at the 90% confidence level, with those derived by using the RS model.

3.5. Spectra of the Central 3' and 6' Regions

In order to examine the reality and the nature of the three spectroscopic components found above, it would help to study their spatial distributions utilizing the imaging capability of ASCA. Accordingly, we have accumulated the GIS and SIS events over two concentric circular regions of smaller radii of 3' (0.6 kpc) and 6' (1.2 kpc), centered on the nucleus, as performed in subsection 3.1 for the 12' region. We again subtracted the blank-sky background spectra. As presented in figure 6, the GIS/SIS spectra accumulated over these regions are similar in shape to those derived from the 12' region (figure 5), and have actually been reproduced successfully by the LMXB+2RS model. The derived parameters, summarized in table 2, are close to those found in the 12' accumulation region (table 1).

In table 3, we show the spatially-dependent luminosities of the three spectral components constituting the LMXB+2RS model. Thus, the three components are statistically significant in every pair of spectra. All the three components are clearly extended, but are more concentrated toward the nucleus than is expected for a uniform distribution. While the luminosities of the LMXB component and the softest (0.3 keV RS) component are consistent with having the same spatial distribution, there is a marginal evidence that the hotter (0.9 keV RS) component is less

extended around the nucleus. All these results reinforce the reality of the three spectral components.

3.6. Alternative Modelings of the X-ray Binary Component

Although we have thus successfully decomposed the spatially-integrated M31 spectra, the LMXB model employed to represent the X-ray binary contribution had been developed for the most luminous LMXBs with luminosity exceeding $\sim 2 \times 10^{37}$ erg s $^{-1}$ (Mitsuda et al. 1984; Makishima et al. 1989a; Asai et al. 2000), residing in our Galaxy and the Large Magellanic Cloud (specifically, LMC X-2). Less luminous LMXBs tend to show more power-law like spectra due to Comptonization (e.g., Mitsuda et al. 1989). Furthermore, there is a claim, though without physical grounds, that LMXBs might exhibit a prominent soft excess component of which the strength is correlated with environmental metallicity (Irwin & Sarazin 1998; Irwin & Bregman 1999ab). With these in mind, we re-fitted the 0.6–10 keV GIS/SIS spectra for the 12' region, but this time by replacing the LMXB model with a single thermal Bremsstrahlung (Bremss for short) model or a single power-law (PL for short) model. In logarithmic plots, the Bremss model is more convex than the PL model, but less convex than the LMXB model (see Appendix for detail). We again fix the absorption to the Galactic value.

As summarized in table 4, the single Bremss model could not reproduce the 0.6–10 keV GIS/SIS spectra due to the soft excess. Adding an RS component (again with the abundance fixed at 1.0 solar) improved the fit significantly, and further adding a second RS component has made the fit acceptable; the obtained Bremss+2RS fit is shown in figure 7a. These results, together with the obtained RS parameters, are basically similar to those we obtained using the LMXB model in table 1. This is understandable, because the Bremss model of the temperature $kT_B \sim 10$ keV is similar in shape to the LMXB model over the ASCA band, except that the former predicts a slightly higher flux below ~ 1.5 keV. However, the LMXB+2RS model reproduces the overall data better than the Bremss+2RS model (with $\chi^2/\text{d.o.f.} = 300/309$ vs. $307/311$), and the difference is significant at a $> 97\%$ confidence level according to an F -test. These results are consistent with the conclusion of Paper I that the 2–20 keV spectrum of M31 is represented significantly better by the LMXB model than the Bremss model.

As to the PL modeling, the fit remained unacceptable even adding up to two RS components (table 4). The unsuccessful PL+2RS fit is shown in figure 7b, where both instruments consistently reveal a negative residual feature near 1.2 keV. This is because the PL model overpredicts the continuum at this energy. In short, the PL model is inappropriate as a representation of the X-ray binary spectrum in M31, as already revealed in Paper I.

4. Discussion

Using the ASCA data, we have confirmed that the spatially integrated 0.6–10 keV X-ray emission from the central regions of M31 comprises three spectral components; the integrated X-ray binary component, and the 0.9 keV (hotter) and the 0.3 keV (cooler) RS components. All the three components are spatially extended, in agreement with the repeated detections of unresolved, possibly diffuse, soft X-ray emission (Trinchieri & Fabbiano 1991; Primini et al. 1993; Supper et al. 1997; West et al. 1997; Trinchieri et al. 1999; Borozdin & Priedhorsky 2000; Primini et al. 2000; Garcia et al. 2000b; Shirey et al. 2001). Below, we compare our results with those from other missions, and discuss the nature of the three components.

4.1. The Binary Component

The integrated binary component dominates the spectrum above ~ 1.5 keV, as already known previously (e.g., Paper I; Trinchieri et al. 1999). We have successfully modeled this emission using our physical LMXB model, consisting of a DBB component and a BB component. This result agrees with the main achievement of Paper I, that the 2–20 keV Ginga spectrum of the whole M31 is described successfully using the same model. Our parameters for the LMXB component are consistent with those derived in Paper I. Furthermore, when integrated up to 12', the 0.5–10 keV luminosity of this component measured with ASCA (2.6×10^{39} erg s $^{-1}$; table 3) compares reasonably with the 2–20 keV luminosity of the whole M31 derived with Ginga, 5×10^{39} erg s $^{-1}$ (Paper I).

We are of course aware that our LMXB model, which has primarily been developed for very luminous ones, may not necessarily be appropriate for fainter sources which must contribute to the spatially integrated ASCA spectra. The spectra of such fainter LMXBs, with luminosities below $\sim 1 \times 10^{37}$ erg s $^{-1}$, may be described better by a PL model with a mild high-energy turn over (Mitsuda et al. 1989). Nevertheless, the luminosity function of discrete X-ray sources in M31 obtained with ROSAT (West et al. 1997) indicates that the integrated X-ray luminosity of M31 is predominantly contributed by sources more luminous than $\sim 1 \times 10^{37}$ erg s $^{-1}$, with the fainter ones contributing only 10% or less. Furthermore, M31 does not host apparent examples of enigmatic “ultra-luminous compact X-ray sources” (ULXs; Makishima et al. 2000) that shine extremely beyond the Eddington limit for a neutron star. Consequently, the largest contribution to the total X-ray emission is thought to come from LMXBs, justifying the use of our LMXB spectral model.

In contrast to our approach, other investigators mostly model the binary component in more conventional ways, in terms of either the Bremss or the PL model (Trinchieri et al. 1999; Irwin & Bregman 1999b; Borozdin & Priedhorsky

2000; Shirey et al. 2001). The Bremss modeling may be consistent with our ASCA data, but evidently this has no physical grounds. Furthermore, the Bremss model has been rejected by the 2–20 keV Ginga spectrum of the whole M31 (Paper I), presumably because this energy band is more suited than the ASCA band to characterize the overall spectral shape of luminous point X-ray sources. The PL modeling has been revealed to be inconsistent with the high-quality ASCA data. We thus conclude that our LMXB model gives the most appropriate account of the integrated binary emission from M31.

To confirm the above idea, we simulated the XMM-Newton EPIC spectrum for bright point sources in M31 (blue one in fig. 7 of Shirey et al. 2001), employing the best-fit PL model of photon index 1.82 and absorption $N_{\text{H}} = 6.7 \times 10^{20} \text{ cm}^{-2}$ as reported by Shirey et al. (2001), and using a publicly available EPIC response (mos1_medium_all_qe17_rmf3_tel5_15.rsp). When fitted with our LMXB model over the 0.6–7.0 keV range, the simulated spectrum exhibits a weak soft excess below ~ 0.8 keV, yielding $\chi^2/\text{d.o.f.} = 446/226$. This meets our expectation, since the spectrum must inevitably contain a small amount of background/foreground diffuse emission, even though it was accumulated over small radii ($10'' - 30''$; Shirey et al. 2001) around bright point sources. The soft excess thus revealed is modeled reasonably well ($\chi^2/\text{d.o.f.} = 288/262$) by two RS components of one solar abundances, with temperatures of $0.91^{+0.18}_{-0.05}$ keV and $0.23^{+0.02}_{-0.03}$ keV. When normalized to the binary component, the inferred luminosities of the two RS components are $\sim 30\%$ of those found from the ASCA spectra. This is reasonable, because the data integration area used to generate the EPIC point-source spectrum is estimated to have a filling factor of 10–40%, as judging from Shirey et al. (2001).

4.2. The Hotter RS Component

The second component, the ~ 0.9 keV thin-thermal plasma emission, is a new component which has not been detected so far by other missions. For example, the Chandra and XMM-Newton observations clearly revealed the presence of apparently diffuse X-ray emission in the central region of M31 (Primini et al. 2000; Garcia et al. 2000b; Shirey et al. 2001). Shirey et al. (2001) decomposed the spectrum of this unresolved emission obtained by XMM-Newton into a soft thin-thermal plasma component of a temperature ~ 0.35 keV, and a hard residual emission from fainter discrete sources. However, they did not find the 0.9 keV thin-thermal plasma which we have discovered.

This discrepancy, we believe, is again due to the difference in the way of modeling the residual binary component contributing to the unresolved emission. Shirey et al. (2001) modeled the residual component in terms of the PL model, which as well as the Bremss is steeper in the soft X-ray range than our LMXB model (Appendix). As a result, the 0.9 keV component in the diffuse emission was presumably taken up by the model describing the binary contribution. Actually, when we replace the LMXB model by the Bremss model in the ASCA spectral fit, the normalization (and hence luminosity) of the 0.9 keV component decreases to $\sim 70\%$ of its original value, although it does not vanish. Furthermore, when the binary contribution to the ASCA spectra is represented by a PL model, the normalization of the 0.9 keV component reduces to $\sim 40\%$ of that found with the LMXB modeling (the fit becoming unacceptable; subsection 3.6, figure 7b, table 4). By Chandra with its excellent imaging capability, the same region was resolved into more point sources than those by XMM-Newton, and the contribution of them to the unresolved emission can be further reduced. However, there have not yet been any detailed spectral analyses but for a hardness ratio one which confirmed the value is consistent with that expected from a ~ 0.3 keV RS component (Primini et al. 2000; Garcia et al. 2000b).

We can independently strengthen the reality of the 0.9 keV component, by considering atomic emission lines. As described in subsection 3.3, the ASCA spectra bears a statistically significant ionized S-K line; so does the diffuse-component spectrum obtained with the XMM-Newton EPIC (red one in fig. 7 of Shirey et al. 2001). Since the S-K lines cannot be emitted significantly by plasmas of temperatures as low as 0.3–0.4 keV, the data require a considerably higher plasma temperature. Furthermore, a close look at the same XMM-Newton EPIC spectrum for the diffuse emission reveals Mg-K (at 1.50 keV) and Si-K (at 2.04 keV) lines of hydrogen-like species. Such an ionization state also require a plasma temperature of ~ 1 keV.

The 0.9 keV component in M31 reminds us of the fact that two large-scale diffuse Galactic X-ray emission phenomena, namely the Galactic ridge emission (Koyama et al. 1986; Kaneda et al. 1997; Valinia & Marshall 1998) and the Galactic bulge emission (Kokubun 2001), both involve a soft component expressed by thin-thermal plasma emission of a temperature 0.6–0.8 keV. These soft components in the Galactic ridge and bulge emission, integrated over the whole Galaxy, exhibit a 0.5–10 keV luminosity of $\sim 4 \times 10^{39} \text{ erg s}^{-1}$ and $\geq 7 \times 10^{37} \text{ erg s}^{-1}$, respectively. Considering our limited data integration region around the M31 nucleus and the measured luminosity, the 0.9 keV RS component of M31 may be similar to the soft component of the Galactic diffuse X-ray emission. Although the origin of these Galactic soft components is still unsettled, an assembly of old supernova remnants may be a possibility (Koyama et al. 1986; Kaneda et al. 1997; Valinia & Marshall 1998). If so, the 0.9 keV RS component in M31 may be related to the past supernova activity in M31.

4.3. The Cooler RS Component

The softest spectral component that appears in the energy range below ~ 0.8 keV has been modeled by a thin-thermal emission with a temperature ~ 0.3 keV, even though there may be a room for alternative modelings. Although the nucleus of M31 emits very soft X-rays, its 0.3–7 keV luminosity, $\sim 4.0 \times 10^{37}$ erg s $^{-1}$ (Garcia et al. 2000a), falls by an order of magnitude below that of our softest component. Furthermore, our softest component is clearly extended (subsection 3.5). Therefore, contribution from the M31 nucleus is considered negligible.

We tentatively consider the softest component as coming from an optically-thin plasma of a temperature ~ 0.3 keV. This agrees with the Chandra and XMM-Newton results on M31, and on NGC 4697 (Sarazin et al. 2001). One obvious candidate for this cooler RS component is warm inter-stellar medium, as has been confirmed in some external galaxies (e.g., Sarazin et al. 2001).

Another promising candidate is an assembly of stellar coronae. A solar-type star has a typical coronal temperature of ~ 0.3 keV, and an X-ray luminosity 5–7 orders of magnitude lower than its bolometric luminosity (e.g., Pallavicini et al. 1981). The integrated bolometric luminosity of M31 is $\sim 1 \times 10^{44}$ erg s $^{-1}$ (Tully 1988), and that from the central 12' region is estimated to be $\sim 4 \times 10^{43}$ erg s $^{-1}$. The measured luminosity of the 0.3 keV RS component (table 3) thus becomes $\sim 6 \times 10^{-6}$ when normalized to the stellar bolometric luminosity therein. Since this value is close to those found for individual coronal sources, the cooler RS component may be contributed significantly by the stellar coronae, as well as by warm inter-stellar medium.

Appendix. Model of the LMXB spectra

The X-ray spectra of luminous ($\gtrsim 2 \times 10^{37}$ erg s $^{-1}$) LMXBs are described successfully with the two-component physical model by Mitsuda et al. (1984), consisting of a softer and a harder components. The softer one is a DBB model, which represents the integrated emission from an optically-thick accretion disk around the nonmagnetized neutron star (Hoshi 1984; Inoue & Hoshi 1987). The harder one is a ~ 2 keV BB model, which represents the emission from the central neutron-star surface where the kinetic energy of the accreting matter is thermalized. The X-ray spectra of LMXBs are hence described by four parameters; the innermost disk temperature T_{in} and the normalization of the DBB component, and the temperature T_{BB} and the normalization of the BB component. Luminous Galactic LMXBs exhibit rather narrow scatter both in kT_{in} and kT_{BB} , typically $kT_{\text{in}} = 0.7 - 1.5$ keV and $kT_{\text{BB}} = 1.3 - 2.5$ keV. The two constituent components usually cross over at energies of 3–7 keV (Mitsuda et al. 1984). This model has been verified against the LMXB spectra taken with various satellites, including Tenma (Mitsuda et al. 1984), Ginga (Makishima et al. 1989a), and ASCA (Asai et al. 2000).

As a specific example, we fitted the spectrum of 4U 1820 – 30 taken with the ASCA GIS in October 1993. This is a typical Galactic LMXB located in the globular cluster NGC 6624, and exhibits a relatively low line-of-sight absorption. It was hence used in Paper I as a comparison source. Since the source is too bright for the SIS, we use the GIS data only. We screened the GIS (GIS2 and GIS3) events as in section 2, to archive a net exposure of ~ 16 ks. The 0.7–10 keV count rate was ~ 99 c s $^{-1}$ per GIS detector, corresponding to ~ 120 mCrab which is typical of 4U 1820 – 30. The spectrum has such a high statistics that the calibration uncertainty becomes the dominant source of errors in the model fitting. We therefore added a systematic error of 1% to each bin of the GIS spectrum. For background, we used a source free region of the same observation with the same radius. Figure 8 shows the background subtracted GIS spectrum without removing the instrumental response.

We fitted the 0.7–10 keV GIS spectrum of this LMXB with our LMXB model, as well as the two conventional models, a single Bremss or a single PL model. We left the absorption column density free. The LMXB model has reproduced the spectrum very well, in spite of the very high signal statistics (figure 8a, table 5). On the contrary, the other two models showed poorer results (figure 8b and c, table 5). The Bremss fit, marginally acceptable, yielded $N_{\text{H}} \sim 2 \times 10^{21}$ cm $^{-2}$ and $kT_{\text{B}} \sim 10$ keV. These values are typical when an LMXB spectrum is approximated by a Bremss model (Makishima et al. 1989a). In this case, the absorption is thought to be artificial, required by the slope of the Bremss continuum (~ 1.4 in the energy range $E \ll kT_{\text{B}}$) which is steeper than that of the DBB model ($\sim \frac{2}{3}$ for $E \ll kT_{\text{in}}$). The temperature obtained through the Bremss fit to the M31 spectrum is close to those for 4U 1820 – 30.

Although the LMXB fit is acceptable, the derived N_{H} is lower than the Galactic value of 1.5×10^{21} cm $^{-2}$ (from Einline and W3nH). This is probably due to a very weak “soft excess” component, emitted by 4U 1820 – 30 itself or environment. Actually, adding an RS model of a temperature ~ 0.9 keV has made the LMXB fit even better, and this model is acceptable even when the absorption is fixed at the Galactic value (table 5). The obtained flux in the 0.5–10 keV energy band of this soft component (2×10^{-10} erg cm $^{-2}$ s $^{-1}$) is only $\sim 2\%$ of that of the LMXB component (1×10^{-8} erg cm $^{-2}$ s $^{-1}$). Therefore, this effect is much weaker than the excess soft X-ray emission observed from M31.

References

Asai, K., Dotani, T., Nagase, F., Mitsuda, K. 2000, ApJS, 131, 571

Borozdin, K. N., Priedhorsky, W. C. 2000, ApJ, 542, L13

Burke, B. E., Mountain, R. W., Harrison, D. C., Bautz, M. W., Doty, J. P. 1991, IEEE Trans. Ele. Dev., 38, 1069

Garcia, M. R., Murray, S. S., Primini, F. A., Forman, W. R., McClintock, J. E., Jones, C. 2000a, *ApJ*, 537, L23

Garcia, M. R., Murray, S. S., Primini, F. A., Forman, W. R., Jones C., McClintock J. E. 2000b, *astro-ph*, 0012387

Gendreau, K. C., Bautz, M., Ricker, G. 1993, *Nucl. Instr. Meth. Phys. Res.*, A355, 318

Hoshi, R. 1984, *PASJ*, 36, 785

Inoue, H., Hoshi, R. 1987, *ApJ*, 322, 320

Irwin, J. A., Bregman, J. N. 1999a, *ApJ*, 510, L21

Irwin, J. A., Bregman, J. N. 1999b, *ApJ*, 527, 125

Irwin, J. A., Sarazin, C. L. 1998, *ApJ*, 499, 650

Kaastra, J. S. 1992, *An X-Ray Spectral Code for Optically Thin Plasmas* (Internal SRON-Leiden Report, updated version 2.0, Leiden)

Kaneda, H., Makishima, K., Yamauchi, S., Koyama, K., Matsuzaki, K., Yamasaki, N. Y. 1997, *ApJ*, 491, 638

Kokubun, M. 2001, PhD. Thesis, University of Tokyo

Koyama, K., Makishima, K., Tanaka, Y., Tsunemi, H. 1986, *PASJ*, 38, 121

Liedahl, D. A., Osterheld, A. L., Goldstein, W. H. 1995, *ApJL*, 438, L115

Makishima, K., Ishida, M., Ohashi, T., Dotani, T., Inoue, H., Mitsuda, K., Tanaka, Y., Turner, M. J. L., Hoshi, R. 1989a, *PASJ*, 41, 531

Makishima, K., Kubota, A., Mizuno, T., Ohnishi, T., Tashiro, M., Aruga, Y., Asai, K., Dotani, T., Mitsuda, K., Ueda, Y., Uno, S., Yamaoka, K., Ebisawa, K., Kohmura, Y., Okada, K. 2000, *ApJ*, 535, 632

Makishima, K., Ohashi, T., Hayashida, K., Inoue, H., Koyama, K., Takano, S., Tanaka, Y., Yoshida, A., et al. 1989b, *PASJ*, 41, 697 (Paper I)

Makishima, K., Tashiro, M., Ebisawa, K., Ezawa, H., Fukazawa, Y., Gunji, S., Hirayama, M., Idesawa, E., et al. 1996, *PASJ*, 48, 171

Mewe, R., Gronenschild, E. H. B. M., van den Oord, G. H. J. 1985, *A&AS*, 62, 197

Mewe, R., Lemen, J. R., van den Oord, G. H. J. 1986, *A&AS*, 65, 511

Mitsuda, K., Inoue, H., Koyama, K., Makishima, K., Matsuoka, M., Ogawara, Y., Suzuki, K., Tanaka, Y., et al. 1984, *PASJ*, 36, 741

Mitsuda, K., Inoue, H., Nakamura, N., Tanaka, Y. 1989, *PASJ*, 41, 97

Ohashi, T., Ebisawa, K., Fukazawa, Y., Hiyoshi, K., Horii, M., Ikebe, Y., Ikeda, H., Inoue, H., et al. 1996, *PASJ*, 48, 157

Pallavicini, R., Golub, L., Rosner, R., Vaiana, G. S., Ayres, T., Linsky, J. L. 1981, *ApJ*, 248, 279

Primini, F. A., Forman, W., Jones, C. 1993, *ApJ*, 410, 615

Primini, F., Garcia, M., Murray, S., Forman, W., Jones, C., McClintock, J. 2000, in *The Interstellar Medium in M31 and M33*, ed Berkhuijsen, E., Beck, R. (Shaker Verlag, Aachen) p145

Raymond, J. C., Smith, B. W. 1977, *ApJS*, 35, 419

Sarazin, C. L., Irwin, J. A., Bregman, J. N. 2001, *ApJ*, in press (*astro-ph* 0104070)

Shirey, R., Soria, R., Borozdin, K., Osborne, J. P., Tiengo, A., Guainazzi, M., Hayter, C., La Palombara, N., et al. 2001, *A&A*, 365, L195

Supper, R., Hasinger, G., Pietsch, W., Truemper, J., Jain, A., Magnier, E. A., Lewin, W. H. G., van Paradijs, J. 1997, *A&A*, 317, 328

Tanaka, Y., Inoue, H., Holt, S. S. 1994, *PASJ*, 46, L37

Trinchieri, G., Fabbiano, G. 1991, *ApJ*, 382, 82

Trinchieri, G., Israel, G. L., Chiappetti, L., Belloni, T., Stella, L., Primini, F., Fabbiano, P., Pietsch, W. 1999, *A&A*, 348, 43

Tully, R. B. 1988, *Nearby Galaxies Catalog* (Cambridge University Press, Cambridge)

Valinia, A., Marshall, F. E. 1998, *ApJ*, 505, 134

West, R. G., Barber, C. R., Folgheraiter, E. L. 1997, *MNRAS*, 287, 10

Yamashita, A., Dotani, T., Bautz, M., Crew, G., Ezuka, H., Gendreau, K., Kotani, T., Mitsuda, K. et al. 1997, *IEEE Trans. Nuc. Sci.*, 44, 847

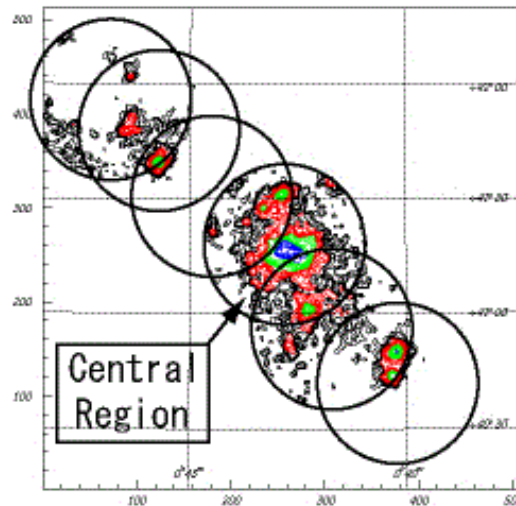


Fig. 1. The GIS2 images of six pointings onto M31, in the energy range of 0.7–10 keV. Each of the six circles represents the field of view of the GIS one pointing. The background is included, and the contours are logarithmically spaced. Sky coordinates are J2000. The present paper is concerned only with the central pointing.

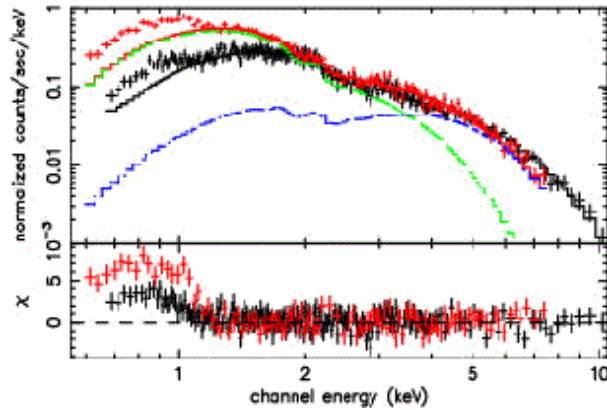


Fig. 2. Background-subtracted GIS (black) and SIS (red) spectra of the central 12' region of M31, presented without removing the instrumental response. They are fitted simultaneously in the energy range above 1.5 keV, with the canonical LMXB model. The green and blue lines represent the DBB and BB model components contributing to the SIS spectrum, respectively. The best fit model is extrapolated to below 1.5 keV, to highlight the soft excess.

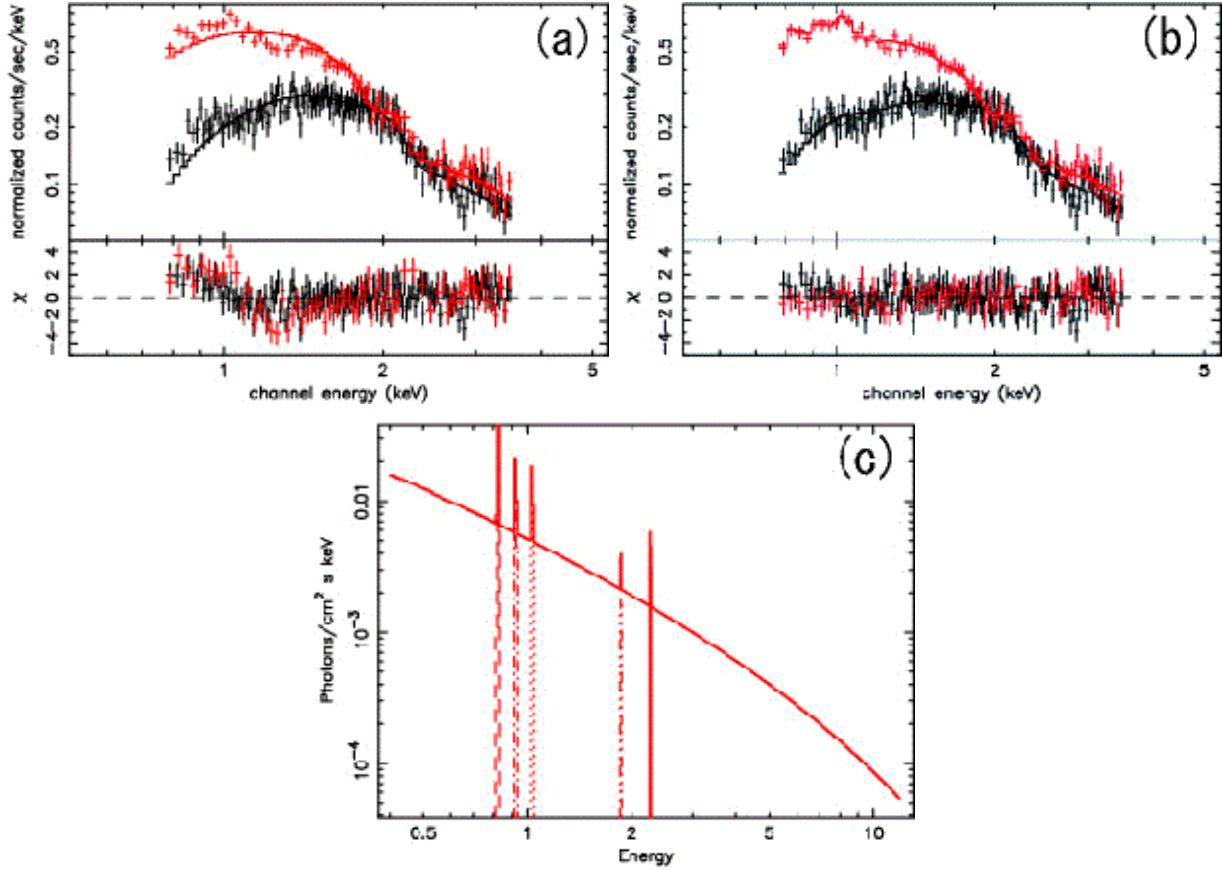


Fig. 3. Spectra of the central $12'$ region of M31, presented over a restricted 0.8–3.5 keV energy band. The data are the same between the two panels. (a) Fitted jointly with a single bremsstrahlung model. (b) Five narrow Gaussians are added, to represent ionized Ne-K, Fe-L, Si-K, and S-K lines. The line parameters are given in text. (c) The incident model corresponding to the fit in panel b.

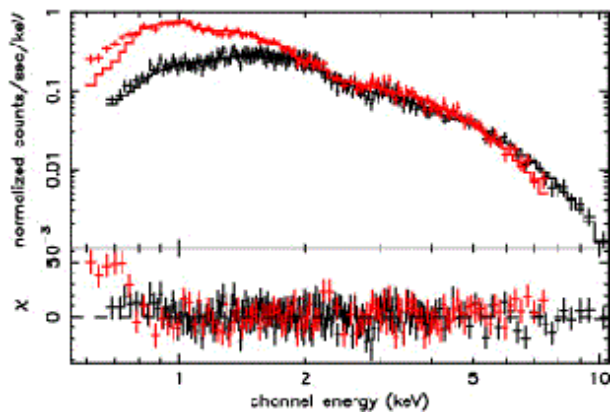


Fig. 4. The same as figure 2, but the simultaneous model fits are performed over the 0.8–10 keV energy range using the LMXB+RS model. The best fit model is extrapolated to below 0.8 keV, to reveal yet another soft excess component.

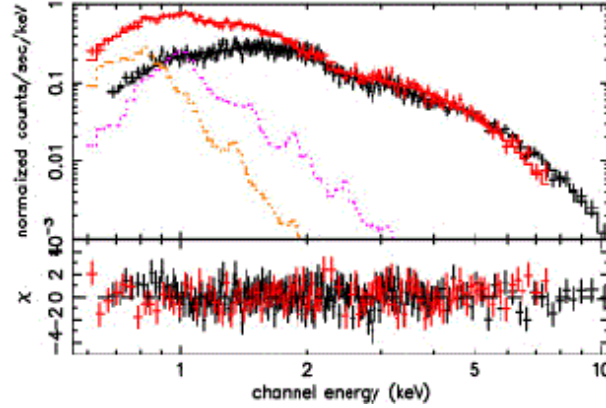


Fig. 5. The same as figure 2, but the model fits are performed over the full 0.6–10 keV energy range using the LMXB+2RS model. The pink and orange lines represent the 0.9 keV and 0.3 keV RS model components contributing to the SIS spectrum, respectively.

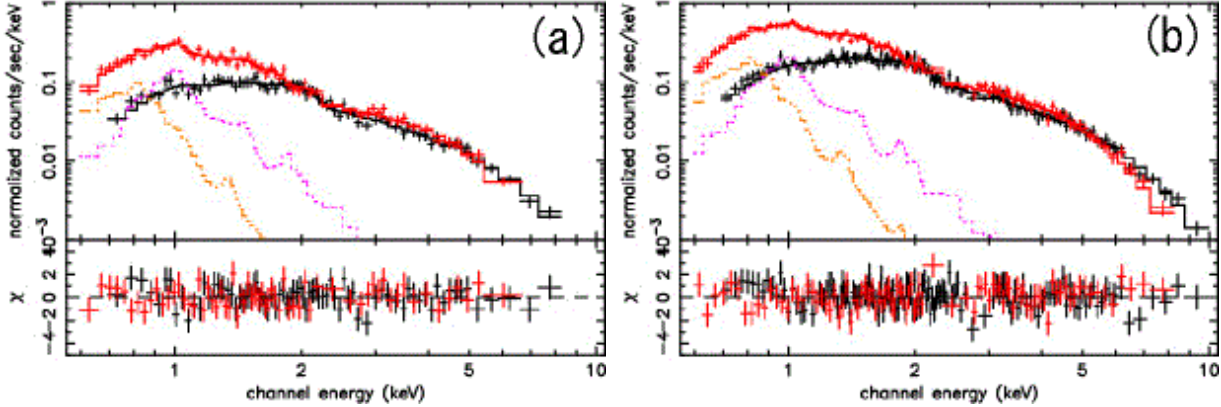


Fig. 6. Spectra of the central 3' (panel a) and 6' (panel b) regions fitted with the LMXB+2RS model over the full 0.6–10 keV energy band, presented in the same way as figure 5.

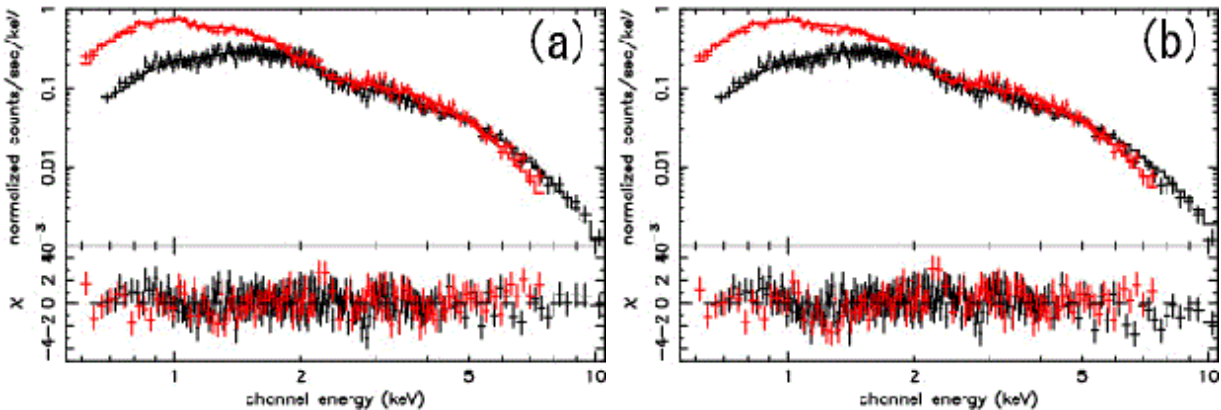


Fig. 7. The same as figure 5, but fitted with (a) the Bremss+2RS model, and (b) the PL+2RS model.

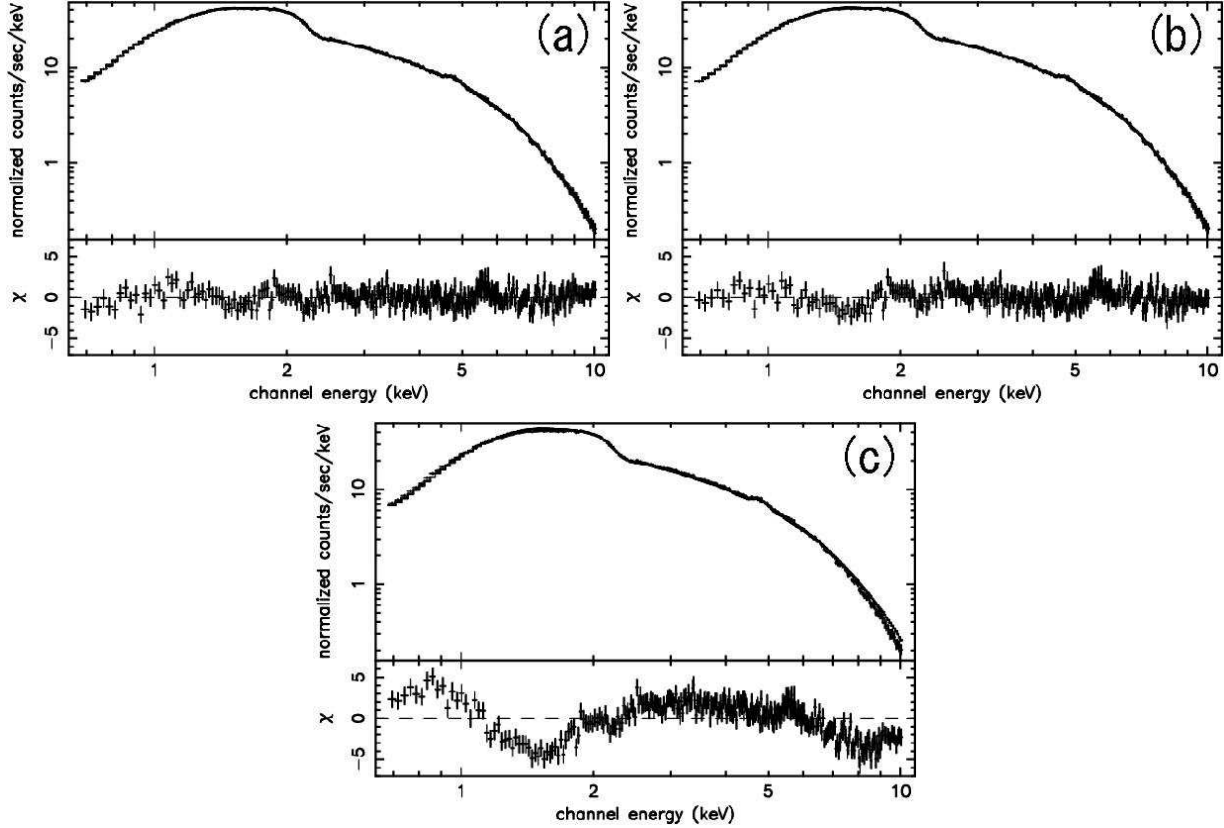


Fig. 8. Background-subtracted GIS spectrum of 4U 1820–30 in the 0.7–10 keV energy band. The data are the same among the three panels. The spectrum is fitted with (a) the LMXB model, (b) a single Bremss model, and (c) a single PL model.

Table 1. Spectral fit results for the central 12' region of M31.*,†

Range and Model	LMXB		$kT_{\text{RS}}^{\ddagger}$	$kT_{\text{RS}}^{\ddagger}$	$\chi^2/\text{d.o.f.}$
	$kT_{\text{in}}^{\ddagger}$	$kT_{\text{BB}}^{\ddagger}$			
1.5–10 keV					
LMXB	0.85 ± 0.09	$1.9_{-0.2}^{+0.3}$	208/221
0.8–10 keV					
LMXB	0.47 ± 0.03	$1.29_{-0.06}^{+0.07}$	534/303
LMXB+RS [§]	$0.94_{-0.09}^{+0.10}$	$2.0_{-0.2}^{+0.4}$	0.79 ± 0.03	...	289/301
0.6–10 keV					
LMXB	$0.41_{-0.03}^{+0.02}$	1.20 ± 0.05	580/313
LMXB+RS [§]	0.72 ± 0.06	$1.7_{-0.2}^{+0.1}$	0.33 ± 0.03	...	372/311
LMXB+2RS [§]	$0.9_{-0.1}^{+0.2}$	$2.0_{-0.3}^{+0.4}$	$0.94_{-0.07}^{+0.10}$	$0.28_{-0.04}^{+0.03}$	300/309

* N_{H} is fixed at the Galactic value of $6.7 \times 10^{20} \text{ cm}^{-2}$.

† All the errors are single-parameter 90% confidence limits.

‡ Temperatures are all in the unit of keV.

§ The metal abundance of the RS component is fixed at 1.0 solar.

Table 2. Results of the LMXB+2RS model fits for the central 3' and 6' regions in the 0.6–10 keV energy band.*

Radius	LMXB		kT_{RS}	kT_{RS}	$\chi^2/\text{d.o.f.}$
	kT_{in}	kT_{BB}			
3'	$0.9_{-0.2}^{+0.5}$	$1.6_{-0.3}^{+2.1}$	$0.95_{-0.08}^{+0.10}$	0.28 ± 0.04	105/130
6'	$0.9_{-0.1}^{+0.2}$	$1.8_{-0.2}^{+0.5}$	$0.94_{-0.08}^{+0.11}$	0.29 ± 0.04	196/219

* The analysis conditions are the same as those for table 1.

Table 3. Luminosities of the three components for different accumulation radii around the nucleus.*,†

Radius	LMXB component	Hotter RS component	Cooler RS component
3'	$7.4^{+0.1}_{-0.2}$ (1)	$0.8^{+0.2}_{-0.1}$ (1)	$0.7^{+0.2}_{-0.1}$ (1)
6'	16.2 ± 0.3 (2.20 ± 0.06)	$1.2^{+0.3}_{-0.2}$ (1.50 ± 0.46)	$1.5^{+0.1}_{-0.3}$ (2.0 ± 0.5)
12'	$26.0^{+0.4}_{-0.6}$ (3.5 ± 0.1)	$1.7^{+0.3}_{-0.4}$ (2.0 ± 0.6)	$2.3^{+0.3}_{-0.2}$ (3.2 ± 0.7)

* The luminosities are in the 0.5–10 keV band, in 10^{38} erg s $^{-1}$.

† The numbers in parentheses are the ratios to the values for the 3' radius.

Table 4. Alternative modelings of the 0.6–10 keV spectra of M31 for the central 12' region.*

Models	$kT_B^\dagger/\Gamma^\ddagger$	kT_{RS}^\dagger	kT_{RS}^\dagger	$\chi^2/\text{d.o.f.}$
Bremss [§]	5.9	683/315
Bremss+RS	$7.4^{+0.5}_{-0.4}$	0.35 ± 0.03	...	364/313
Bremss+2RS	$8.6^{+0.9}_{-0.5}$	$0.90^{+0.12}_{-0.05}$	0.28 ± 0.04	307/311
PL	1.79 ± 0.02	455/315
PL+RS	$1.71^{+0.03}_{-0.02}$	$0.35^{+0.07}_{-0.04}$...	362/313
PL+2RS	$1.68^{+0.02}_{-0.03}$	0.9 ± 0.1	$0.31^{+0.06}_{-0.07}$	348/311

* The fitting conditions are the same as those for table 1.

† All temperatures are in keV.

‡ Γ is the PL photon index.

§ Errors are not shown because of the poor fit.

Table 5. Spectral fit results for the GIS spectrum of 4U 1820 – 30.*,†

Models	N_H^\ddagger	kT_{in}^\S	kT_{BB}^\S	kT_B^\S	Γ^\P	kT_{RS}^\S	$\chi^2/\text{d.o.f.}$
LMXB	6.5 ± 0.7	0.99 ± 0.02	$1.92^{+0.05}_{-0.03}$	283/297
Bremss	16.3 ± 0.4	$9.6^{+0.1}_{-0.2}$	329/299
PL	31	1.76	...	1463/299
LMXB+RS	15 (fixed)	$0.92^{+0.02}_{-0.01}$	1.86 ± 0.03	0.86 ± 0.03	307/296

† A systematic error of 1% is added to each data bin.

* Errors refer to 90% confidence limits, but are not shown if $\chi^2/\text{d.o.f.} > 2$.

‡ N_H is in 10^{20} cm $^{-2}$.

§ All temperatures are in keV.

¶ Γ is the PL photon index.

|| The metal abundance is fixed at 1.0 solar.